A SEMI-ANALYTICAL DESCRIPTION OF TWO-PHASE FLOW NEAR PRODUCTION WELLS IN HYDROTHERMAL AND GEOPRESSURED RESERVOIRS

John W. Pritchett
Systems, Science and Software
P. O. Box 1620, La Jolla, California 92038

Two-phase flow, in which gas and liquid water coexist within the pores, generally occurs in geothermal reservoirs in one of two ways. First, gravity segregation can cause the formation of a gas or steam cap near the top of the aquifer with single-phase liquid conditions prevailing at deeper levels. Second, within the liquid zone, production-induced pressure drop can cause the formation of a two-phase region adjacent to a production well in which both phases flow horizontally towards the well. If such a two-phase region forms, classical formulae which relate production rate to aquifer thickness, permeability, well diameter, fluid viscosity, and pressure drop no longer apply. The presence of a two-phase region will substantially increase the net resistance to fluid flow, reducing the production rate for a given downhole pressure.

In liquid-dominated geothermal reservoirs, two distinct regimes are of principal interest. First, in hydrothermal systems, liquid water will boil due to production-induced pressure drop if the local pressure reaches the vapor pressure for the reservoir temperature. As pressure further declines, the temperature will begin to drop according to the saturation curve for water/steam mixtures, and the steam volume fraction ("steam saturation") will increase. Second, in geopressured systems such as those that underlie the Gulf Coast region, reservoir pressures typically exceed vapor pressure by hundreds of bars, so that steam will never form. However, geopressured reservoir fluids typically contain large quantities of dissolved natural gas, principally methane. Since the solubility of gases in water increases with pressure for a given temperature, the pressure drop induced by production may cause the evolution of free gas from solution, again creating a two-phase zone near the well.

On time-scales which are large compared to those associated with compressibility-induced pressure transients, the flow in the neighborhood of a well may be regarded as essentially steady. For example, for the special case of a fully penetrating well in a homogeneous reservoir of constant thickness, if the flow is single-phase-liquid the classical linear relation between pressure and the logarithm of radial distance from the well may be shown to apply. For two-phase flow, the problem is much more complicated even if steady radial flow is assumed. Strong nonlinearities arise both from the relative permeability functions employed and from the constitutive description of the two-phase fluid mixture. In general, to solve the resulting problem, resort must be had to laborious numerical integration procedures based upon the laws of mass, momentum, energy and species conservation which incorporate the relevant constitutive data (i.e., the steam tables and the appropriate gas solubility and P-V-T data).

In the present paper, certain constitutive approximations are introduced in analytical form for both cases of interest (water/steam and water/

gas). It is demonstrated that these approximations, when combined with the basic conservation laws, yield a much simpler set of equations in each case consisting of a single algebraic equation, a single ordinary integral, and the prescribed relative permeability data. It is further shown that the resulting equations are of the same form for both cases (water/steam and water/gas) so that they may be solved by the same procedures. Although numerical methods are still needed to solve the integral, an enormous simplification compared to the general case has been achieved. Finally, comparisons between results for the present simplified scheme and results generated by numerical integration of the basic equations show that the simplified scheme, in spite of the relatively crude constitutive assumptions employed, is entirely adequate for engineering purposes.

To develop the simplified theory, we start by considering steady horizontal fluid flow which is one-dimensional in the sense that all physical variables are to be determined as functions of a single scalar space variable x. Flow rates are generally high near wells, so we will neglect the effects of both heat conduction and capillarity. The fluid consists of a mixture of H_2O and one additional chemical species. Flows of this type are governed by the following conservation laws (see, for example, Pritchett, et al., 1975; Garg, et al., 1977a; Garg and Pritchett, 1977b):

Mass Conservation:

$$A\,(\rho_G\,U_G + \rho_L\,U_L) = Q \tag{1}$$

Energy Conservation:

$$A\,(\rho_G\,H_G\,U_G + \rho_L\,H_L\,U_L) = QH_F \tag{2}$$

Conservation of Second Species:

$$A\,(\rho_G\,C_G\,U_G + \rho_L\,C_L\,U_L) = QC_F \tag{3}$$

Gas Momentum Conservation (Darcy Law):

$$U_G + \frac{k\,R_G}{\rho_G\,\nu_G}\,\frac{dP}{dx} = 0 \tag{4}$$

Liquid Momentum Conservation (Darcy Law):

$$U_L + \frac{k\,R_L}{\rho_L\,\nu_L}\,\frac{dP}{dx} = 0 \tag{5}$$

In these expressions:

$A = A(x)$ = prescribed cross-sectional area distribution

$k = k(x)$ = prescribed absolute permeability distribution

Q = constant = mass flow rate (mass per unit time)

H_F = constant = flowing enthalpy (energy per mass)

C_F = constant = flowing second species mass fraction.

The principal unknowns are functions of x:

$\rho_G(\rho_L)$ = gas (liquid) mass density

$U_G(U_L)$ = gas (liquid) volume flux

$H_G(H_L)$ = gas (liquid) enthalpy

$C_G(C_L)$ = mass fraction of second species in gas (liquid) phase

$\nu_G(\nu_L)$ = gas (liquid) kinematic viscosity

P = fluid pressure.

Finally, R_L and R_G are the prescribed relative permeability functions for the liquid and gas phases, respectively. These are ordinarily provided as functions of the gas saturation S (the gas phase volume fraction). We will hereafter assume that R_L may be equivalently regarded as a function of R_G, with the usual properties:

$$R_L\ (R_G = 0) = 1$$

$$R_L\ (R_G = 1) = 0$$

$$R_L' = \frac{dR_L}{dR_G} < 0 \quad \text{for} \quad 0 < R_G < 1.$$

The basic conservation laws (Eqs. 1-5) may be manipulated to yield the equivalent set:

Pseudopressure Definition:

$$P^* = P_0 - Q \int_{x_0}^{x} \left(\frac{\nu_L}{Ak}\right) dx \qquad (6)$$

Mass Conservation:

$$\int_{P_0}^{P} \left(\frac{\nu_L}{\nu_G} R_G + R_L \right) dP = P^* - P_0 \qquad (7)$$

Energy Conservation:

$$\nu_G R_L (H_F - H_L) = \nu_L R_G (H_G - H_F) \qquad (8)$$

Second Species Conservation:

$$\nu_G R_L (C_F - C_L) = \nu_L R_G (C_G - C_F). \qquad (9)$$

It should be noted that, in these expressions, the liquid and gas volume fluxes (U_L and U_G) no longer appear. Two new constants (P_0, x_0) and one new space variable (P^*) remain to be defined. If Q is positive, it follows that P must monotonically decrease with x; for negative Q, P monotonically increases with x. Since for both flashing (water/steam) and bubbling (water/soluble gas) systems the gas volume fraction declines with increasing pressure, at some point in space (x_0) a pressure will be reached (P_0) at which the gas phase vanishes. Beyond this point, the flow will be single-phase liquid. Hereafter, the subscript "0" will be used to denote conditions at this "boiling point" (x_0).

The "pseudopressure" (P^*) is a function of x, and may be simply defined, within the two-phase region, as the pressure which would prevail if two-phase effects were absent. Beyond the two-phase region ($x > x_0$ for $Q < 0$), of course, $P = P^*$. Within the two-phase region, the true pressure (P) will generally be smaller than P^*. Now, the determination of $P^*(x)$ is usually a fairly straightforward problem. In radial flow towards a fully-penetrating well with constant rock permeability and constant aquifer thickness, for example, we have $A = 2\pi hx$ where h is aquifer thickness, $k = k_0$, $\nu_L = \nu_{L0}$ so that Eq. (6) yields the classical result:

$$P^* = P_0 - \frac{Q\nu_{L0}}{2\pi k_0 h} \ln (x/x_0) .$$

The treatment for non-constant permeability, thickness, etc. is only slightly more complicated. In other words, the "pseudopressure" (P^*) may be used as an alternative to x as an independent variable; within the two-phase region, if the variables of genuine interest (P, R_L, R_G, H_L, H_G, etc.) can be determined as a function of P^*, Eq. (6) provides the necessary map to physical space. Therefore, the essential physical problem for the two-phase region is posed by Eqs. (7), (8) and (9). These equations relate

the true pressure (P) to the pseudopressure (P*) subject to the constants of the problem (P_0, H_F, C_F), the prescribed relative permeability function $R_L(R_G)$, and the constitutive data which provides ν_L, ν_G, H_L, H_G, C_L and C_G. The solution of this problem is quite formidable, in general. As will be shown, however, the introduction of judiciously chosen constitutive assumptions can simplify the mathematical problem considerably, while retaining adequate accuracy for engineering purposes.

We first consider the case of a fluid consisting of pure H_2O. In the single-phase region of the flow, the fluid temperature is known (T_0) so that the boiling pressure (P_0) may be obtained using the steam tables (see Meyer, et al., 1967) which provide the saturation pressure as a function of temperature. The steam tables also provide the enthalpy and kinematic viscosity for both water and steam (H_{L0}, H_{G0}, ν_{L0}, ν_{G0}) at the boiling point (T_0, P_0). Within the two-phase region, we will now assume that the kinematic viscosity for the liquid phase is essentially constant, and that the gas-phase kinematic viscosity is inversely proportional to absolute pressure, as would be the case for an ideal gas. The steam tables also show that the enthalpy of saturated steam is almost independent of temperature (or pressure) over a wide range. Finally, we will assume that the liquid-phase enthalpy is proportional to temperature and that the saturation pressure/temperature relation for saturated water/steam may be locally linearized. Thus, the constitutive assumptions for the water-steam case are:

$$\nu_L(P) = \nu_{L0} = \text{constant} \tag{10}$$

$$\nu_G(P) = \nu_{G0}\, P_0/P \tag{11}$$

$$H_G(P) = H_{G0} = \text{constant} \tag{12}$$

$$H_L(P) = H_{L0} + c_v\, \gamma(P - P_0) \tag{13}$$

where we define:

$c_v = (dH_L/dT)$ at P_0 on saturation line

$\gamma = (dT/dP)$ at P_0 on saturation line.

Next, we will consider a physical situation in which the fluid consists of a mixture of H_2O and a slightly soluble gas such as methane or carbon dioxide. Such a flow will be essentially isothermal. We assume that pressures are sufficiently high that steam will not evolve; thus, the gas phase will consist of pure gas (no water vapor). Again, we assume

that the liquid-phase kinematic viscosity is constant and that we are treating an ideal gas so that the gas phase kinematic viscosity is inversely proportional to pressure. Finally, we assume that the solubility of the gas in water is governed by Henry's law, which means that the liquid-phase gas species concentration declines in proportion to pressure. Also, the bubbling pressure (P_0) can be related to the gas-species concentration in the single-phase region through Henry's constant, which may be regarded as a function of temperature (T_0).

Thus, we have, for the water/gas case:

$$\nu_L(P) = \nu_{LO} = \text{constant} \tag{14}$$

$$\nu_G(P) = \nu_{GO}\, P_0/P \tag{15}$$

$$C_G(P) = 1 = \text{constant} \tag{16}$$

$$C_L(P) = C_{LO}\, P/P_0. \tag{17}$$

The analysis for the water/steam case is accomplished by introducing the constitutive assumptions (Eqs. 10-13) into the mass (Eq. 7) and energy (Eq. 8) conservation relations. Similarly, for the water/soluble gas case, we combine Eqs. (14)-(17) with the mass (Eq. 7) and species (Eq. 9) relations. After substantial algebraic manipulation, both cases may be expressed by the following:

$$\frac{P}{P_0} = \frac{\nu_{GO}\, R_L}{\nu_{GO}\, R_L + \nu_{LO}\, \zeta\, R_G} \tag{18}$$

$$\frac{P^*}{P_0} = 1 - \nu_{LO}\nu_{GO}\zeta \int_0^{R_G} \frac{R_L\,(R_L - R_G\, R_L')[\nu_{GO}\, R_L + \nu_{LO}\,(\zeta + 1)\, R_G]}{(\nu_{GO}\, R_L + \nu_{LO}\, \zeta\, R_G)^3}\, dR_G \,. \tag{19}$$

The difference between the two cases arises from differences in P_0, ν_{GO}, and ν_{LO} for a given value of single-phase temperature T_0 (and, for the water/gas case, the value of C_{LO}), and from the definition of the dimensionless constant ζ. For water/steam, ζ is given by:

$$\zeta_{WS} = (H_{GO} - H_{LO})/c_v \gamma P_0 \tag{20}$$

and for the water/soluble gas case,

$$\zeta_{WG} = (1 - C_{LO})/C_{LO} \cdot \qquad (21)$$

Note that, for the water/steam case, ζ depends only on the single-phase region temperature T_0; for the water/gas case, ζ depends only upon C_{LO}, the single-phase region gas species mass fraction.

Thus, the solutions of Eqs. (18) and (19) will depend on the character of the relative permeability function $R_L(R_G)$, on the ratio ν_{GO}/ν_{LO} and on the value of ζ. For the water/steam case, these latter two parameters, in turn, depend only on the single-phase region temperature (T_0); for the water/gas case, they depend on the nature of the gas and its mass fraction in the single-phase region as well as upon temperature. The values of these dimensionless parameters tend to be very different for the two cases, as illustrated in the following table. For the water/gas case, we have chosen methane as the gas species and have considered mass fractions of 0.005 and 0.01 for illustrative purposes. For temperatures of geothermal interest, the values are as follows:

	Water/Steam			Water/Methane					
				$C_{LO} = 0.005$			$C_{LO} = 0.01$		
T_0(°C)	P_0 (bar)	$\frac{\nu_{GO}}{\nu_{LO}}$	ζ	P_0 (bar)	$\frac{\nu_{GO}}{\nu_{LO}}$	ζ	P_0 (bar)	$\frac{\nu_{GO}}{\nu_{LO}}$	ζ
200	15.6	12.9	9.0	298	1.2	199	824	0.9	99
220	23.2	9.7	7.7	249	1.5	199	686	1.0	99
240	33.5	7.4	6.5	216	1.9	199	577	1.1	99
260	46.9	5.7	5.4	190	2.4	199	497	1.3	99
280	64.2	4.4	4.4	170	3.0	199	438	1.5	99
300	85.9	3.4	3.5	154	3.5	199	385	1.8	99
340	146.0	2.1	1.8	---	---	---	---	---	--
374.15*	221.0	1.0	0.0	---	---	---	---	---	--

Finally, to obtain particular solutions, the relative permeability function $R_L(R_G)$ must be specified. For illustrative purposes, we will hereafter adopt the Corey formulation (see Corey, et al., 1956). Solutions to Eqs. (18) and (19), expressed in terms of the relation between "pseudopressure" P* and true pressure P, are shown in Figure 1 for the water/steam case and in Figure 2 for the water/methane case (with C_{LO}, the single-phase methane mass fraction, equal to 0.01). These solutions were obtained by straightforward numerical integration of Eqs. (18) and (19), subject to the constitutive data listed above and to the Corey relative permeability curves.

*Critical point.

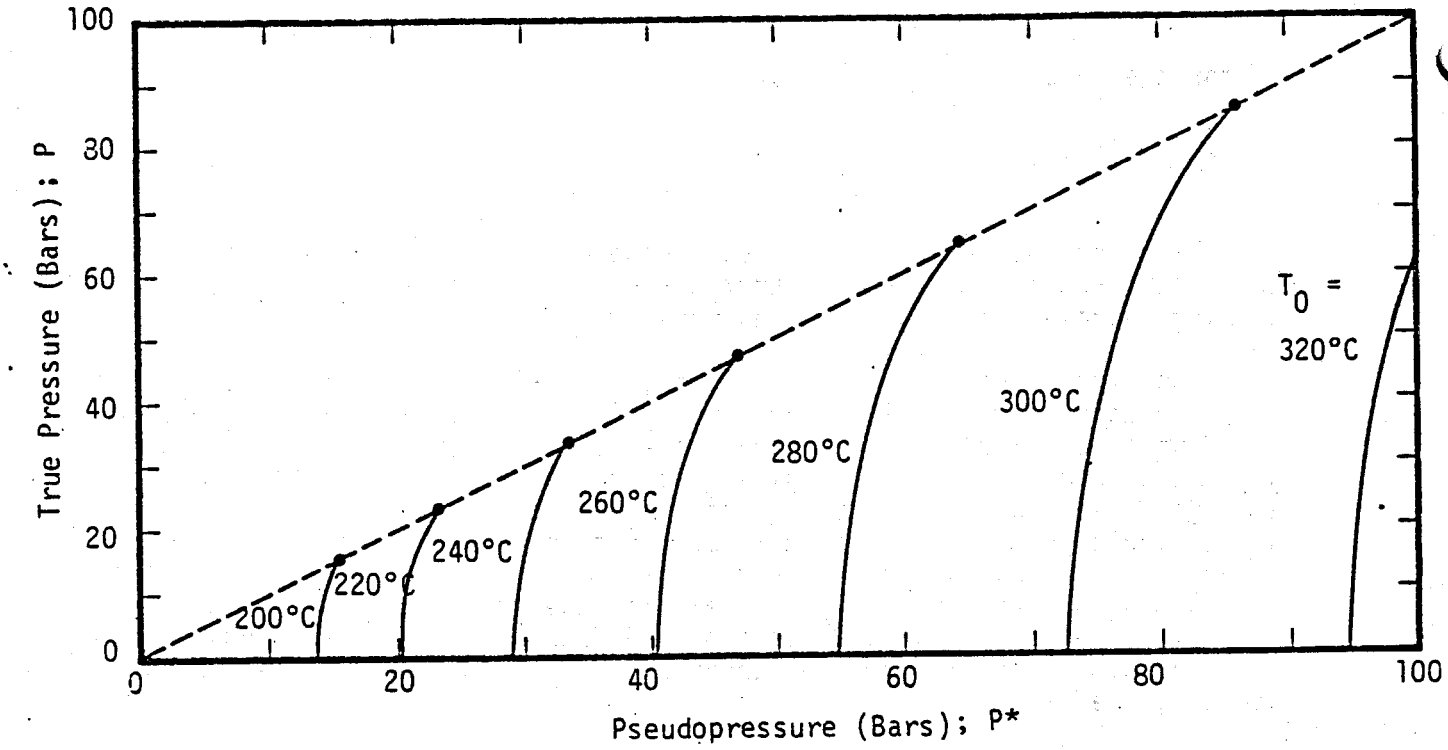

Figure 1. Water/steam case -- true pressure (P) as a function of "pseudo-pressure" (P*) for Corey relative permeabilities and for various single-phase region temperatures (T_0).

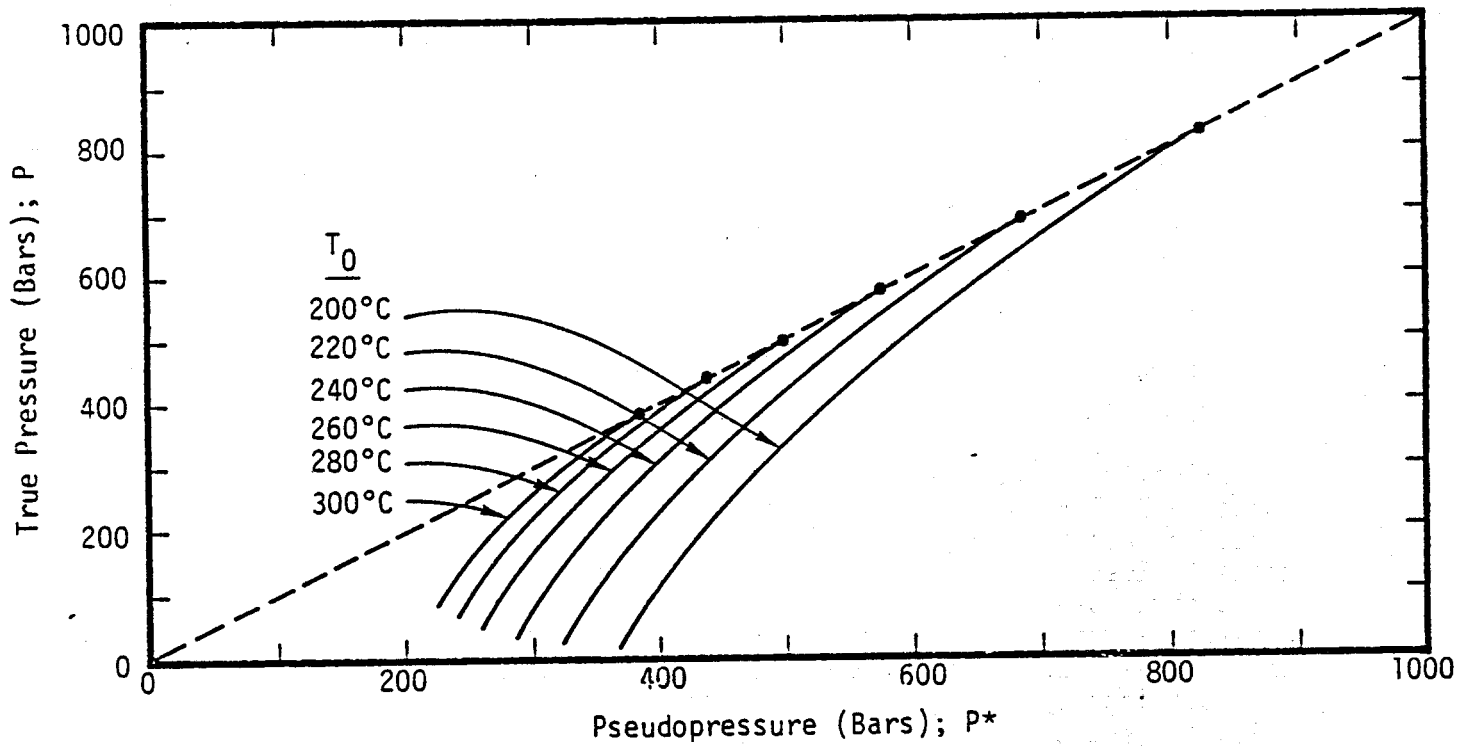

Figure 2. Water/methane case -- true pressure (P) as a function of "pseudo-pressure" (P*) for Corey relative permeabilities and for various single-phase region temperatures (T_0) with single-phase region methane mass fraction (C_{L0}) = 0.01.

The relative simplicity of this procedure arises from the constitutive simplifications described previously (Eqs. 10-13 for water/steam; Eqs. 14-17 for water/gas). Despite the crude character of these assumptions, the results are remarkably accurate. To assess the present results, a series of lengthy numerical calculations was carried out based on the original conservation laws (Eqs. 1-5) and using complete constitutive descriptions, based on measurements, for both water/steam and water/methane mixtures. These constitutive packages are described in Pritchett, et al. (1975) and Garg, et al. (1977a), respectively.

Sample results of a few of these test calculations are illustrated in Figure 3. We examine the water/steam case and consider a fully-penetrating well of radius 10 cm in an aquifer 100 meters thick with a uniform horizontal permeability of 100 millidarcies. Corey relative permeabilities are assumed. Five hundred meters from the well, the pressure and temperature are maintained at P_B and T_B, respectively with P_B greater than the vapor pressure associated with T_B so that the boundary lies in the single-phase region. We then pose the following question: how does the sand face pressure at the well vary with the production rate? In Figure 3, results of two such sets of calculations are presented, with the following boundary parameters and associated boiling pressures (P_0):

Problem	P_B	T_B	Vapor Pressure $(T_B) = P_0$
W1	90 bars	300°C	85.9 bars
W2	40 bars	240°C	33.5 bars

The solid curves (for cases W1 and W2) each result from a single integration of Eqs. (18) and (19). The solid circles each represent the results of a brute-force numerical integration of the primitive equations with a complete set of constitutive data as described above. Equally good comparisons have been made for water/methane systems as well.

The excellent agreement between the results of the present simplified approach and those arising from brute-force numerical integration of the exact equations indicates that the constitutive approximations employed (Eqs. 10-13 and 14-17), which express all constitutive parameters in terms of their values at the boiling point (x_0, P_0), are adequate for calculating the steady character of the two-phase flow near a well. The relative simplicity of the resulting technique permits predictions to be made in a straightforward and efficient way of the relations among sand face pressure, reservoir pressure, and production rate for geothermal wells operating in the two-phase regime.

REFERENCES

Corey, A. T., C. H. Rathjens, J. H. Henderson and M. R. J. Wyllie (1956), "Three-Phase Relative Permeability," Trans. AIME, V. 207, p. 349.

Garg, S. K., J. W. Pritchett, M. H. Rice and T. D. Riney (1977a), "U. S. Gulf Coast Geopressured Geothermal Reservoir Simulation," Systems, Science and Software Report SSS-R-77-3147.

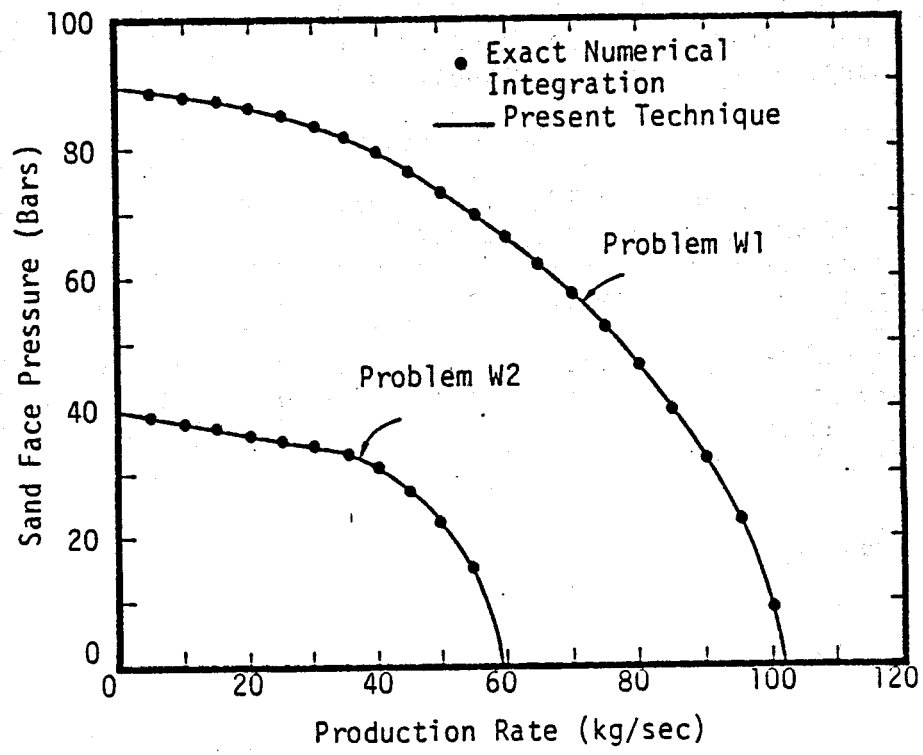

Figure 3. Comparison of present results with solutions obtained without constitutive approximations.

Garg, S. K. and J. W. Pritchett (1977b), "On Pressure-Work, Viscous Dissipation and the Energy Balance Relation for Geothermal Reservoirs," Advances in Water Resources, V. 1, No. 1, pp. 41-47.

Meyer, C. A., R. B. McClintock, G. J. Silvestri and R. C. Spencer, Jr. (1967), 1967 ASME Steam Tables, American Society of Mechanical Engineers, New York.

Pritchett, J. W., S. K. Garg, D. H. Brownell, Jr. and H. B. Levine (1975), "Geohydrological Environmental Effects of Geothermal Power Production -- Phase I," Systems, Science and Software Report SSS-R-75-2733.

GEOTHERMAL RESERVOIR SIMULATIONS WITH SHAFT79

by Karsten Pruess and Ron C. Schroeder

Lawrence Berkeley Laboratory, Berkeley, Ca. 94720

INTRODUCTION

The rational development of geothermal resources requires an adequate knowledge of the behavior of a given reservoir under various production and injection schemes. Mathematical modeling attempts to provide such knowledge and to determine important reservoir parameters, such as formation permeabilities and reserves of fluid and heat.

Because of phase changes and because of the coupling between energy- and mass-flow, the equations describing geothermal reservoirs are strongly non-linear. This limits the applicability of analytical approximations and has motivated the development of numerical simulators. In this paper, we review the concepts and methods used in LBL's geothermal simulator SHAFT79, and illustrate its application to a variety of typical problems.

PHYSICAL MODEL AND SOLUTION METHOD

The simulator SHAFT79 was developed for computing two-phase flow phenomena in geothermal reservoirs. The program handles transient initial-value problems with prescribed boundary conditions. SHAFT79 is an improved version of the simulator SHAFT78, which was discussed in detail in ref. 1). It solves coupled equations for mass- and energy-transport, using an integrated finite difference method. This method allows a very flexible description of reservoirs because it does not distinguish between one-, two-, or three-dimensional regular or irregular geometries.

The main assumptions and approximations made in the formulation of SHAFT79 are as follows: (1) Geothermal reservoirs are approximated as systems of porous rock saturated with one-component fluid in liquid and vapor form. (2) All rock properties - porosity, density, specific heat, thermal conductivity, absolute permeability - are independent of temperature, pressure, or vapor saturation. (3) Liquid, vapor, and rock matrix are in local thermodynamic equilibrium, i.e. at the same temperature and pressure, at all times. (4) Capillary pressure is neglected.

The main new feature in SHAFT79 as compared with SHAFT78 is a completely simultaneous, iterative solution of the coupled mass- and energy-transport equations. This allows between ten and one hundred times larger time steps than the sequential method employed in SHAFT78. In particular, phase transitions can be computed accurately and efficiently. SHAFT79 offers a choice of several methods for solving the coupled non-linear equations for mass- and energy-flow. The preferred solution method is fully implicit, employs a Newton/Raphson iteration for simultaneous solution of the non-linear mass- and energy-transport equations, and uses an efficient sparse solver.[2] SHAFT79 has been applied to problems with up to 350 elements in three dimensions. Typical throughputs range from 0.1 in highly transient situations to more than 10^6 in problems approaching steady state. Here throughput is defined as ratio of the fluid mass flowing through the surface of an element in one time step, divided by the fluid mass initially in place in that element.

APPLICATIONS

Table 1 gives an overview of the types of systems and processes which have been modeled with SHAFT79. Below are presented results of selected SHAFT79-simulations which illustrate the range of applications. Parameters for the individual cases are given in the figure captions. Relative permeabilities were obtained from Corey's equations, with residual immobile steam saturation S_{sc} equal to zero, and residual immobile water saturation S_{wc} varying between 0.40 and 0.70.

DEPLETION OF A RESERVOIR WITH SHARP STEAM/WATER INTERFACE

When steam is produced from above a liquid water table, boiling commences near the top of the water zone. This gives rise to a drop in temperature and pressure, whereby a two-phase layer between water and steam zones is established. Water moves upward into the two-phase zone, releasing pressure below the boiling front and advancing it downward.[3] In

GEOMETRY	TYPE OF PROBLEM	SIMULATED PROCESSES
1-D, rectangular	depletion of two-phase geothermal reservoirs[3]	various production and injection schemes for reservoirs with uniform initial conditions or with sharp steam/water interfaces
1-D, cylindrical	two-phase flow near wells	production from two-phase zones; cold water injection into two-phase and superheated steam zones, respectively
2-D, rectangular	Krafla geothermal reservoir (Iceland)[4]	different space and time patterns of production and injection
2-D, cylindrical	high level nuclear waste repository[5]	long-term evolution of temperatures and pressures near a powerful heat source (in progress)
3-D, regular	two-phase interference test in Cerro Prieto (Mexico)	(in progress)
3-D, irregular	Serrazzano geothermal reservoir (Italy)[3]	detailed field production from 1960 to 1966

Table 1: Simulation Studies with SHAFT79.

the examples studied (see fig. 1) the top of the two-phase zone does not dry up until after the boiling front has reached the bottom of the reservoir. This occurs after 6.4 years for the "high permeability" case (A in fig. 1), and after 9.6 years for the "low permeability" case (B in fig. 1). Vapor saturation at the top of the water table then reaches 46.7 % for case A and 78.9 % for case B. Pressure at the steam/two-phase interface, at a depth of 500 m, declines very slowly during the advancing of the boiling front in case A. The reason for this is that the most rapid boiling occurs at the bottom of the two-phase zone. This provides a supply of hotter steam, which flows up from depth and tends to maintain temperature and hence pressure at the top of the two-phase zone. In case B this mechanism for pressure maintenance is much less effective because of the lower permeability.

INJECTION OF COLD WATER

Cold water injection into a steam reservoir gives rise to a hydrodynamic front and, trailing behind it, a temperature front. In the finite-difference simulation of this process subsequent elements undergo phase transitions from superheated steam to two-phase conditions to subcooled water. Fig. 2 shows the fronts at two different times. It is apparent that the fronts are propagated according to the parameter t/R^2. The volume swept by the temperature front is close to 1/4 of the volume swept by the hydrodynamic front. This reflects the fact that, at a porosity of 20 %, the volumetric heat capacity of water is about 1/4 of the volumetric heat capacity of the rock/water mixture.

SIMULATION OF KRAFLA FIELD (ICELAND)

Fig. 3 shows a vertical two-dimensional grid as used by Jonsson for simulating production and injection at Krafla.[4] The reservoir is initially almost entirely filled with liquid water close to saturated conditions. Various production and injection schemes were explored in an attempt to optimize injection, i.e. to combine pressure and temperature maintenance during production with minimal sacrifices in terms of decreasing vapor saturation S. Fig. 4 shows typical results. Jonsson finds that deep injection is preferable to shallow injection. Complete problem specifications and discussions of results are given in ref. 4).

SIMULATION OF SERRAZZANO FIELD (ITALY)

The most complex simulation effort undertaken with SHAFT79 to date is a case study (history match) of the Serrazzano reservoir. Serrazzano is one of the distinct zones of the extensive geothermal area near Larderello in central Tuscany (Italy). Detailed production data gathered since 1939 and an extensive body of geological and hydrological work make Serrazzano an attractive example for developing geothermal reservoir simulation methodology (see references given in 3). Fig. 5 gives a map of the reservoir, and fig. 6 shows the geologically accurate mesh as developed by Weres.[7] Conceptual model of the reservoir and parametrization of the problem are discussed in refs. 3) and 7).

Many parameters are only partially known, and are determined in trial-and-error fashion by comparing simulated reservoir performance with field observations. A valuable criterion for determining absolute permeabilities is that well blocks must remain very close to steady flow conditions. Our most complete simulation so far covers the period from 1960 to 1966. With the permeability distribution as indicated in fig. 5 we achieve steady flow for all wells producing since 1961 or earlier to within 2 % for the entire six year period modeled (i.e., the difference between inflow and production for any well block never exceeds 2 %).

From mass balance considerations it can be shown that most of the fluid reserves in Serrazzano are in place in liquid form. Little is known, however, about the distribution of pore water in the reservoir. Making the tentative assumption that liquid water is distributed throughout most of the reservoir, we compute a pressure decline (see fig. 7) which is slower than observed in the field by a factor of approximately 3.5. In the simulation pressure declines slowly because boiling is spread out over a large volume. We conclude that in most of the reservoir volume no liquid water is present, and we shall modify our initial conditions accordingly in subsequent simulations. We also need to correct some imbalances in initial conditions, which are apparent from the initial non-monotonic behavior of pressure in fig. 7.

CONCLUSION

The simulator SHAFT79 uses efficient methods for computing mass- and energy-transport in geothermal reservoirs, and allows for a flexible description of irregular geometric features. A broad range of applications, including idealized systems as well as large field problems, demonstrates its usefulness for geothermal reservoir studies. Further development work is presently under way to improve on some of the restrictive approximations made in the formulation of the physical model.

ACKNOWLEDGEMENT

This work was supported by the U.S. Department of Energy under contract No. W-7405-ENG-48.

REFERENCES

(1) K. Pruess, J.M. Zerzan, R.C. Schroeder, and P.A. Witherspoon, Description of the three-dimensional two-phase simulator SHAFT78 for use in geothermal reservoir studies, paper SPE-7699, presented at the Fifth Symposium on Reservoir Simulation, Denver/Colorado, 1979.

(2) I.S. Duff, MA28 - a set of Fortran subroutines for sparse unsymmetric linear equations, Report AERE - R 8730, Harwell/Oxfordshire, Great Britain (June 1977).

(3) K. Pruess, G. Bodvarsson, R.C. Schroeder, P.A. Witherspoon, R. Marconcini, G. Neri, and C. Ruffilli, Simulation of the depletion of two-phase geothermal reservoirs, paper SPE-8266, presented at the 54th Annual Fall Technical Conference and Exhibition of the SPE, Las Vegas/Nevada, 1979.

(4) V. Jonsson, Lawrence Berkeley Laboratory Report LBL-10003 (in preparation).

(5) R. Eaton, private communication.

(6) S.K. Garg, Pressure transient analysis for two-phase (liquid water/steam) geothermal reservoirs, paper SPE-7479, presented at the 53rd Annual Fall Technical Conference and Exhibition of the SPE, Houston/Texas, 1978.

(7) O. Weres, A model of the Serrazzano zone, Proc. Third Stanford Workshop on Geothermal Reservoir Engineering, Stanford/California, 1977.

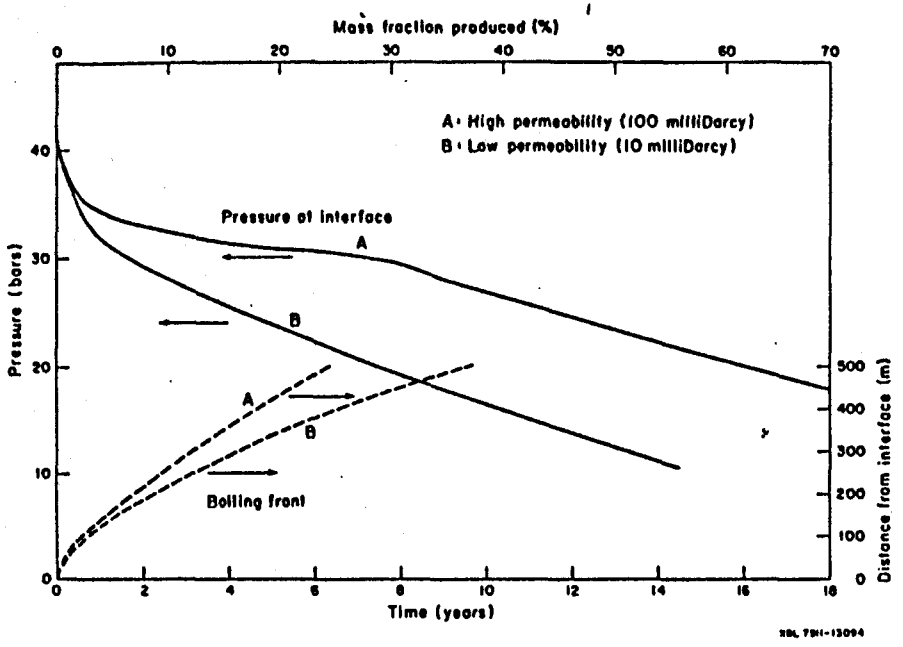

Fig.1: Depletion of a reservoir with sharp steam/water interface. The reservoir is a vertical column of 1 km depth with a volume of 1 km^3 and "no flow" boundaries. For purposes of numerical simulation it is subdivided into 44 horizontal elements. Initially, the bottom half is filled with liquid water, the top half with superheated steam, with temperature T = 252 °C and pressures carefully equlibrated under gravity. (Rock parameters: density = 2000 kg/m^3; specific heat = 1232 J/kg °C; porosity = 10 %; residual immobile water saturation = 70 %) Depletion occurs uniformly at the top with a constant rate of 50 kg/s. The curves are for a permeability of 10^{-13} m^2 (A) and 10^{-14} m^2 (B), respectively. Typical time steps in the simulation are 2 - 5 x 10^6 seconds, corresponding to throughputs of up to 250.

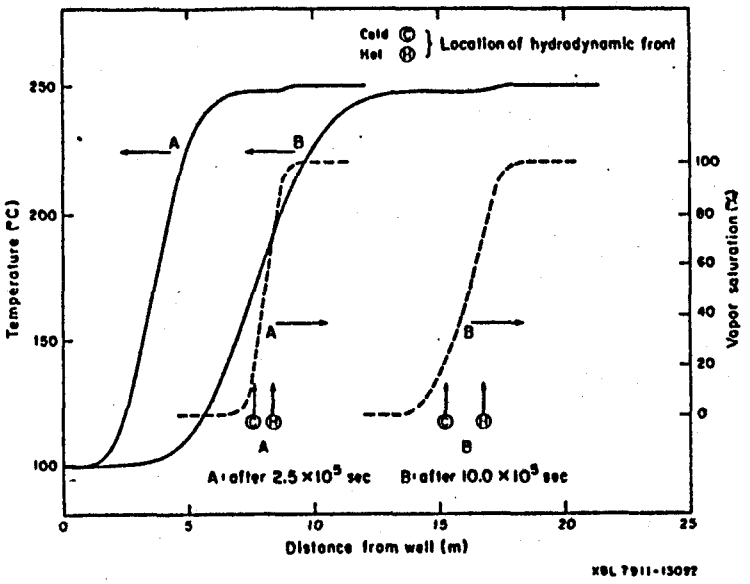

Fig. 2: Injection of cold water into a steam zone. The reservoir is a cylinder with large radius, initially filled with superheated steam at T = 250 °C, pressure = 38 bars. Water with T = 99.3 °C is injected along the center line at a constant rate of 0.14 kg/s m. The numerical simulation employs an axisymmetric grid as used by Garg.[6] (Rock parameters: density = 2650 kg/m^3; specific heat = 1000 J/kg °C; porosity = 20 %; heat conductivity = 5.25 W/m °C; permeability = 10^{-13} m^2; residual immobile water saturation = 40 %) The simulation uses time steps from 2500 to 10000 seconds, with throughputs of up to 6. The arrows labeled C and H show the locations of the hydrodynamic front if all injected water were to remain at injection temperature (C) or were heated up to initial reservoir temperature (H).

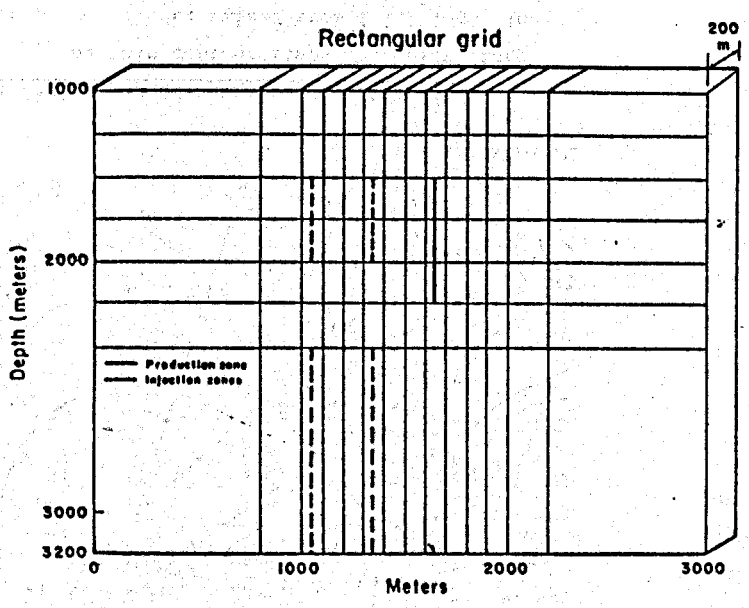

XBL 910-13062

Fig. 3: Two-dimensional grid for simulation of Krafla (Iceland). (from ref. 4)

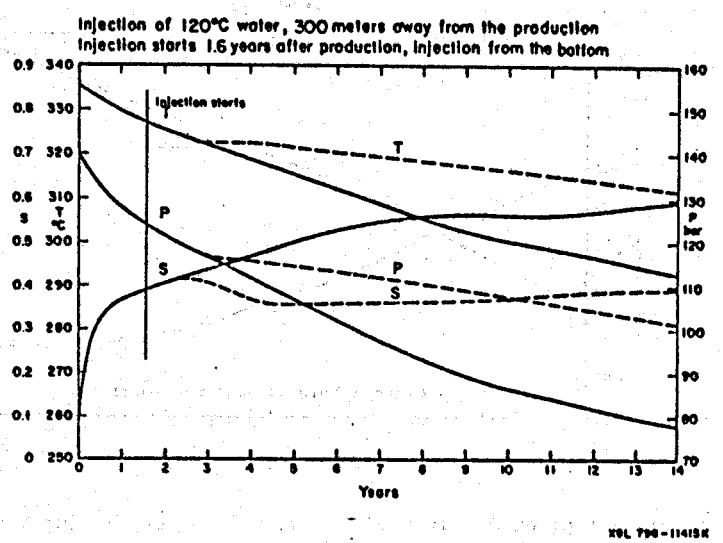

XBL 790-11415A

Fig. 4: Simulated performance of Krafla reservoir. Temperature, pressure and vapor saturation at the well block are given as function of time with injection (dashed lines) and without injection (solid lines). Production rate is 45 kg/s and injection rate is 22.5 kg/s. Typical time steps in the simulation are 1.25×10^6 seconds, with throughputs of about 0.1 (from ref. 4).

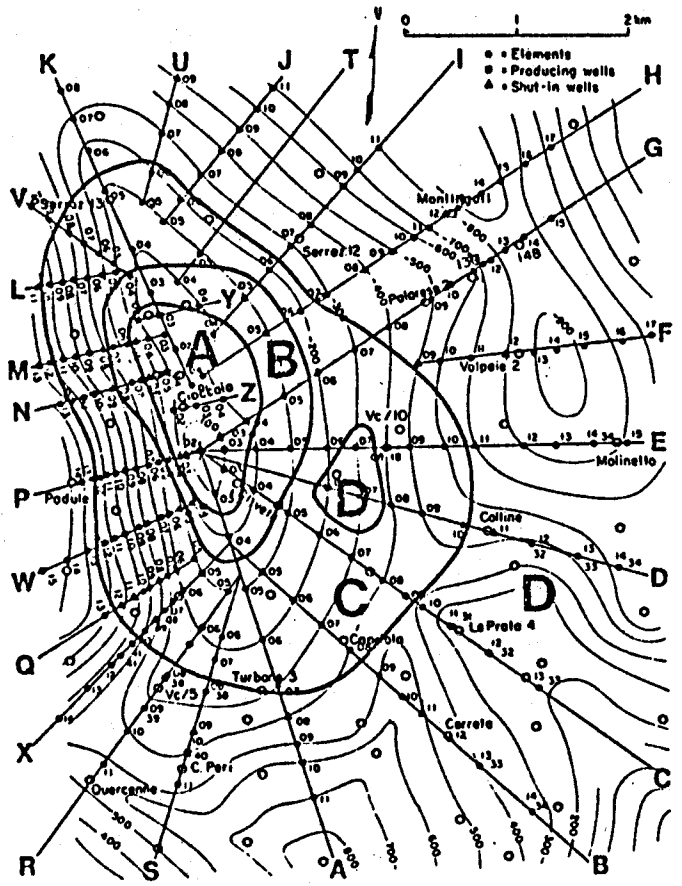

Fig. 5: Aerial map of Serrazzano geothermal reservoir. The thin contour lines show elevations of the cap rock as determined from drill logs. The straight lines labeled A to Z indicate the locations of geological cross sections used in constructing a three-dimensional finite difference grid.[7] Locations of elements (nodes) are also shown. A - D are regions of different permeability as determined in the simulation: A - 0.75×10^{-12} m^2; B - 0.25×10^{-12} m^2; C - 0.75×10^{-13} m^2; D - 0.15×10^{-13} m^2.

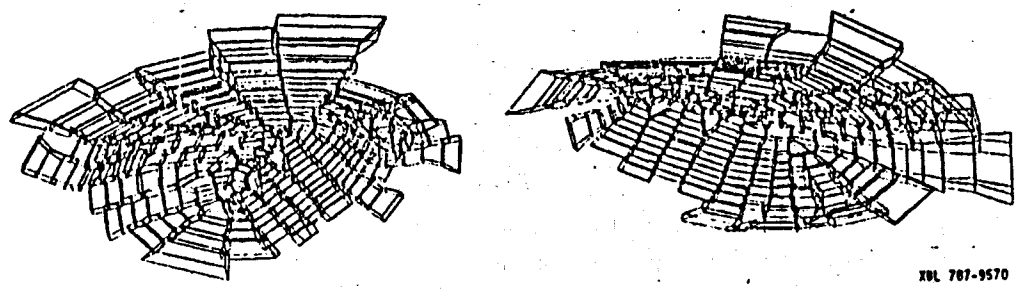

Fig. 6: Serrazzano grid. The computer-generated geologically accurate grid of the Serrazzano reservoir as developed by Weres is shown in two rotated perspective views (ref. 7). This three-dimensional grid represents a reservoir that is a curved thin sheet approximately 1 km from top to bottom, with an aerial extension of about 25 km^2. It has 234 polyhedral elements, with 679 polygonal interfaces between them. There are up to 10 interfaces per element.

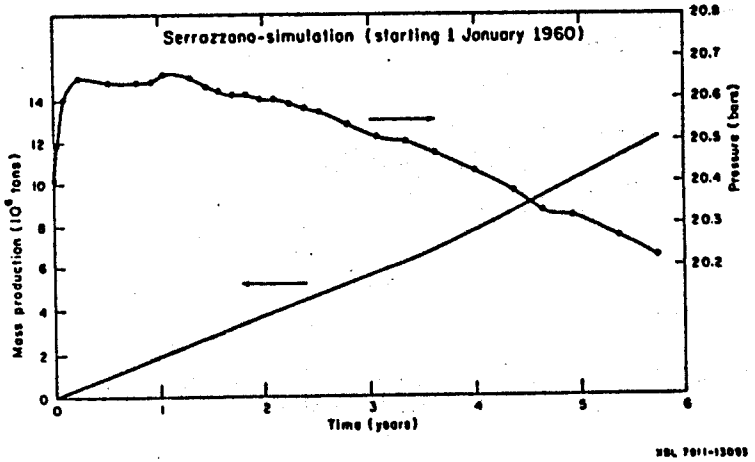

Fig. 7: Average reservoir steam pressure and cumulative fluid production as calculated in Serrazzano simulation. Typical time steps in the simulation are 10 to 50 days, with throughputs of up to 65.